EXAMINING THE POTENTIAL CONTRIBUTIONS OF EXTREME "WESTERN V" SEA SURFACE TEMPERATURES TO THE 2017 MARCH–JUNE EAST AFRICAN DROUGHT

Chris Funk, Andrew Hoell, Sharon Nicholson, Diriba Korecha, Gideon Galu, Guleid Artan, Fetene Teshome, Kinfe Hailermariam, Zewdu Segele, Laura Harrison, Abebe Tadege, Zachary Atheru, Catherine Pomposi, and Diego Pedreros

Anthropogenic warming of Western V sea surface temperatures contributed to East African drought. Extremely warm (FAR = 1) Western V SST doubled the probability of drought, contributing to widespread food insecurity.

INTRODUCTION. During March–June (MAMJ) 2017 East Africa (EA; 35°–50°E, 12°S–9°N) experienced an extensive drought across Tanzania, Ethiopia, Kenya, and Somalia that contributed to extreme food insecurity (Funk et al. 2018, hereafter F18) approaching near-famine conditions (FEWSNET 2017a; FSNAU 2017). Effective forecasts, monitoring, and mitigation by the Intergovernmental Authority on Development (IGAD) Climate Predictions and Applications Centre and international partners (FEWSNET 2017a) motivated effective humanitarian responses. When the 2017 MAMJ rains failed, humanitarian assistance was already arriving, stabilizing food prices (FEWSNET 2017b).

Climate simulations indicate (F18) that strong El Niños may often be followed by exceptional warming in the western Pacific, creating the potential for northeastern Ethiopian/southern African droughts followed by La Niña–like dry conditions during October–December and MAMJ in eastern EA, as in 1999–2001, 2010/11, and 2016/17. While 2016 October–December precipitation deficits do not appear to be significantly influenced by climate change (Uhe et al. 2018), prior research finds that human influence increased the probability of drought during the last severe drought in 2011 (Lott et al. 2013).

Here, we examine EA climate trends and drivers (Fig. 1) and then formally attribute the 2017 EA rainfall deficits and SST extrema (Fig. 2).

EA MAMJ RAINFALL TRENDS. Figure 1a shows standardized EA rainfall anomalies based on the 1900–2014 Centennial Trends (CenTrends; Funk et al. 2015b) dataset and 2015–17 Climate Hazards group Infrared Precipitation with Stations (CHIRPS; Funk et al. 2015c) values. As noted by many authors (Funk et al. 2005; Williams and Funk 2011; Lyon and DeWitt 2012; Nicholson et al. 2012; Funk et al. 2013; Hoell and Funk 2014; Liebmann et al. 2014; Lyon 2014; Nicholson 2014; Yang et al. 2014; Nicholson 2016; Hoell et al. 2017; Liebmann et al. 2017; Nicholson 2017; Funk et al. 2018) and many datasets (Sun et al. 2018), EA has experienced a large increase in the frequency of droughts. Since 1999 only two EA MAMJ seasons were above normal. Figure 1b also shows EA data from the Global Precipitation Climatology Centre (GPCC; Schneider et al. 2014) and a new Ethiopian dataset created by combining CHIRPS with ~150 quality-controlled gauge observations. These also indicate substantial severe declines. Note that the EA region presented is very large and may not be homogeneous across the entire domain

AFFILIATIONS: Funk and Pedreros—U.S. Geological Survey, Earth Resources Observation and Science Center; Funk, Korecha, Galu, Harrison, Pomposi, and Pedreros—University of California Santa Barbara Climate Hazards Center, Physical Sciences Division; Hoell—NOAA Earth Systems Research Laboratory; Nicholson—Florida State University, Department of Meteorology, Earth, Ocean, and Atmospheric Science; Korecha and Galu—Famine Early Warning Systems Network; Artan, Segele, Tadege, and Atheru—Intergovernmental Authority on Development (IGAD) Climate Prediction and Applications Centre; Teshome and Hailermariam—National Meteorological Agency of Ethiopia
CORRESPONDING AUTHOR: Chris Funk, chris@geog.ucsb.edu

DOI:10.1175/BAMS-D-18-0108.1

A supplement to this article is available online (10.1175/BAMS-D-18-0108.2)

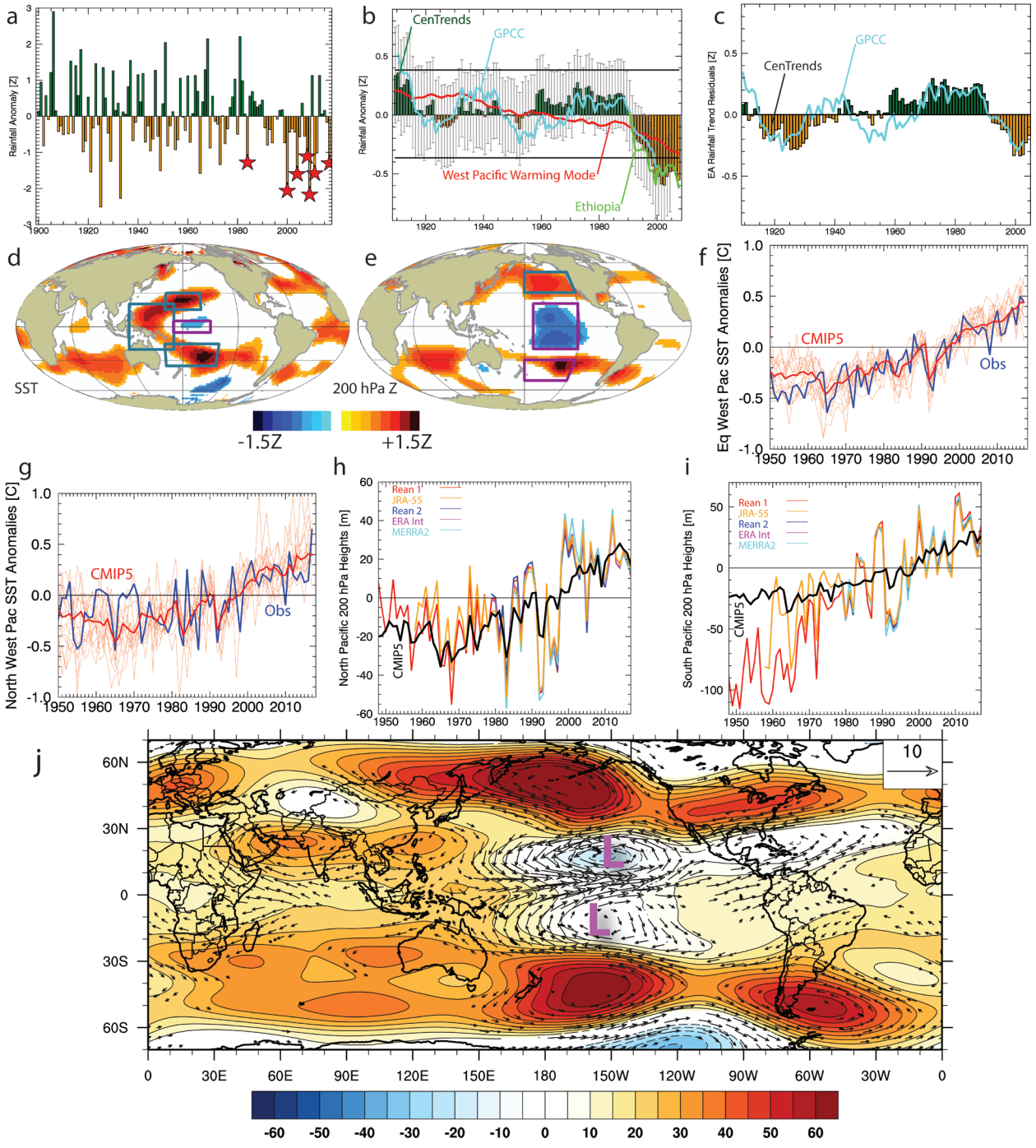

Fig. 1. (a) Standardized EA rainfall from CenTrends/CHIRPS; stars denote droughts. (b) 20-yr EA rainfall with bootstrapped confidence intervals and standard errors. Vertical error bars denote CenTrends kriging standard errors. Horizontal lines indicate deviations significant at $p = 0.05$, based on 10,000 bootstrapped samples. Red line indicates west Pacific warming mode regression estimates. Ethiopia time series averaged over Ethiopia southeast of 9°N, 35°E. (c) EA decadal rainfall decadal variability, based on WPWM regression residuals. (d),(e) Dry season composites of MAMJ SST and Reanalysis I 200-hPa heights. Screened for significance at $p = 0.1$. (f),(g) MAMJ SST time series. (h),(i). MAMJ 200-hPa heights from multiple reanalyses. (j) Changes in CAM5 200-hPa heights and winds during 1981–2016 vs 1921–80 WNP warm events, screened for significance at $p = 0.1$ (Funk et al. 2018).

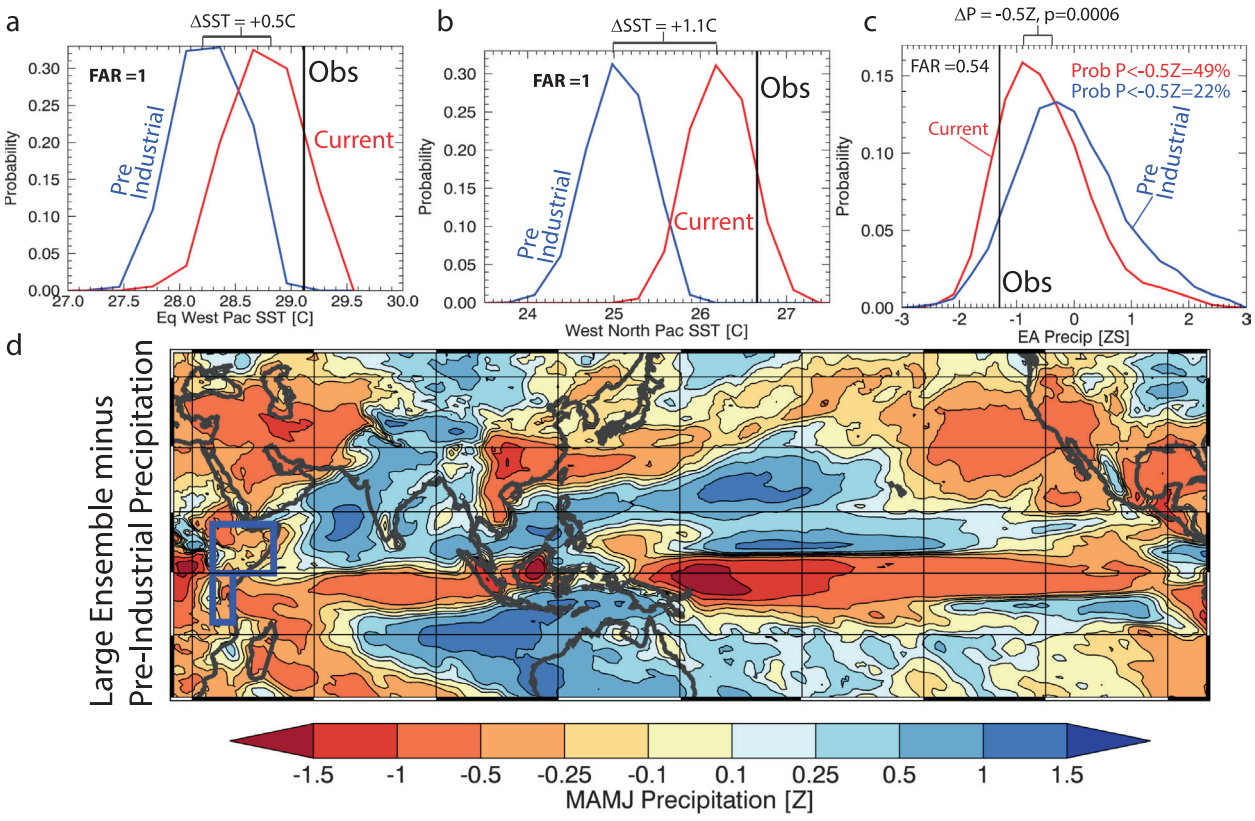

Fig. 2. (a),(b) Preindustrial and 2016–18 distributions for WEP and WNP SST. 2017 ERSSTv4 values are shown with vertical lines. CESM1 SST bias adjusted based on the 1920–2017 LE and observed SST averages. (c) EA precipitation distributions for these same analog seasons. Rainfall based on blue boxes in Fig. 2d. The –0.5Z distribution shift is highly significant (p = 0.0006). (d) A map of the difference in precipitation for the 43 large ensemble analog seasons (WVG < –1Z and Niño-4 values between 0 and 1Z) and 674 preindustrial analogs (Niño-4 values between 0 and 1Z). When strong WVG conditions occur along with neutral-warm Niño-4 SST, we find a La Niña–like response associated with dry EA conditions.

or MAMJ season (Nicholson 2017), but most of this region has experienced substantial declines (Funk et al. 2015b), and analysis of a more homogeneous eastern EA region identifies similar changes (F18).

Several recent studies (Lyon 2014; Yang et al. 2014) have suggested that Pacific decadal variability (Lyon et al. 2014) primarily accounts for the recent decrease in rainfall. These studies, however, are based on analyses of detrended EA precipitation. These trends are large (Funk et al. 2015b; Nicholson 2017) and should not be discounted. The red line in Fig. 1b shows an estimate of the EA rainfall trend based on a regression with the west Pacific warming mode—the first principal component of global SST after the influence ENSO has been removed (Funk and Hoell 2015). It has been shown that increases in this mode have been associated with an enhanced Walker circulation, drying over East Africa, and a characteristic "Western V" Pacific SST warming pattern (Funk and Hoell 2015, 2017). The so-called Western V stretches poleward and eastward from a point near the Maritime Continent (Fig. 1d). Our EA trend estimate indicates a −0.5Z decline between 1900 and 2017 (throughout Z stands for standardized anomaly or Z score). CenTrends and GPCC residuals from this trend mode (Fig. 1c) also exhibit similar and substantial decadal variations. Between 1900–1919 and 1998–2017, the observed EA time series declines from +0.3Z to −0.5Z; ~0.5Z of this decline may be associated with the trend mode, and ~0.3Z may be associated with decadal changes.

We can explore these changes further by compositing (Figs. 1d,e) Extended Reconstructed SST version 4 (ERSSTv4; Huang et al. 2015) standardized MAMJ SSTs and NCEP–NCAR Reanalysis 1 200-hPa heights for recent EA drought years (stars in Fig. 1a). We see a distinct Western V structure and a La Niña–like temperature dipole in ocean temperatures (Fig. 1d). In the upper atmosphere we find La Niña–like upper-level cyclonic lows over the equatorial eastern Pacific. Poleward of these lows we also see upper-level height increases (Fig. 1e). These height gradients produce

vigorous easterly disruptions of the subtropical westerly jet that converge near the date line, enhancing subsidence, decreasing precipitation over the central equatorial Pacific (F18), and enhancing the Indian Ocean branch of the Walker circulation (Williams and Funk 2011; Liebmann et al. 2014, 2017). See upper-level winds and velocity potential changes in Fig. ES1 in the online supplemental material.

Observed SST from the western equatorial Pacific (WEP; 20°S–20°N, 120°–170°E) and western North Pacific (WNP; 13°–30°N, 160°E–140W°) have experienced very large increases (>+0.6Z) since the 1950s (Figs. 1f,g) that track closely with estimates from a multimodel CMIP5 climate change ensemble (see Table ES1 in the online supplemental material). According to ERSSTv4, 2017 MAMJ WEP and WNP SST values were the second warmest or warmest on record. This is consistent with WEP/WNP warming that tends to follow strong El Niños (F18); since 1981, large jumps in west Pacific SST have followed in six out of the eight strongest El Niños. As recently noted (Newman et al. 2018), the 2015/16 El Niño produced exceptionally warm Niño-4 SSTs.

Upper-level midlatitude Pacific height fields from five reanalyses (Figs. 1h,i) indicate enhanced ridging to the northeast and southeast of the Western V SST anomalies. Such ridging would enhance the impact of La Niña–like upper-level equatorial lows, diverting the subtropical westerly jet and increasing subsidence near the date line (Fig. ES1). Composites of the differences in the Community Atmosphere Model version 5 (CAM5) upper-level height and winds (Fig. 1j) during strong versus moderate WNP events (see F18) emphasize how such remote height changes modulate the Walker circulation by enhancing date line subsidence.

These observational results (Fig. 1) indicate that EA MAMJ droughts are associated with warm WNP/WEP SST and stronger Walker circulation anomalies.

SST AND PRECIPITATION ATTRIBUTION. We next use simulations from the Community Earth System Model version 1 (CESM1; Hurrell et al. 2013) to examine WEP/WNP SST extremes and EA rainfall. The CESM1 represents mean SST conditions and ENSO variations well (Flato et al. 2013; Hurrell et al. 2013). CESM1 west Pacific warming trends and the associated negative teleconnection to EA rainfall is similar to that found in observations (Funk and Hoell 2017).

To characterize 2017 WEP and WNP SST, we use 40 "historic" simulations for 2016, 2017, and 2018; these realizations represent a world with climate change. These simulations can be contrasted with simulations representing preindustrial conditions (Figs. 2a,b), identifying substantial warming. Note that that the historic CMIP5 multimodel ensemble also indicates rapid warming in these regions [Figs. 1f,g and Table ES1; see also Table 7 of Funk et al. (2018)]. The influence of climate change, measured by the fraction of attributable risk (FAR), can be defined as FAR = $1 - (P_0/P_1)$, where P_0 is the modeled probability of the event in a climate without anthropogenic influence, and P_1 is the probability in a climate with anthropogenic influence (Allen 2003; Stott et al. 2004). Here, the FAR values are 1 in both cases. These temperature extremes would be extremely unlikely without human-induced climate change.

We next use the CESM1 to explore "Western V gradient" (WVG) impacts. This approach is similar to previous attribution analyses (Funk et al. 2015a) based on the WPG, except that we extend the gradient definition to incorporate the WNP, since extratropical heating and height disruptions (Figs. 1d,e) help intensify the Walker circulation (Fig. 1j), producing subsidence over EA (Fig. ES1). Note that we use the precipitation simulations directly, rather than using a statistical "two-step" approach. The WVG is defined as the standardized difference between Niño-4 and Western V SST: WV = [Z(WEP) + Z(WNP)]/2, where Z() denotes standardization. *The core of our attribution analysis is that we use the modeled EA CESM1 rainfall distributions to evaluate the impact of the WVG.*

Most WVG values since 1999 have been below normal, and the 2017 WVG value was –1.4Z, indicating a strong gradient. The 2017 season, however, stands out as unique, given that it also exhibited warm (+0.8Z) Niño-4 SST conditions. Extreme Western V SST coexisted with modestly warm east Pacific SST (F18). While such a unique event is hard to evaluate using observations, F18 suggests that CESM1 simulations indicate substantial increases in the frequency of very warm west Pacific SSTs (see Fig. 9I in F18), as do all the CMIP5 models (as in Table 7 in F18 and Table ES1 herein). Here we contrast similar events (WVG values of <–1Z and Niño-4 SST between 0 and +1Z; 43 events between 2016 and 2018) with similar preindustrial conditions absent Western-V warming (Niño-4 SST between 0 and +1Z; 674 events).

Examining the precipitation differences, we find a La Niña–like precipitation response (Fig. 2d), despite neutral-warm Niño-4 SST. In the presence of extreme Western V warming we find dry EA conditions, event without cool La Niña SST. Figure 2c expresses this tendency using EA rainfall distributions based on the

43 and 674 2016–18 and preindustrial analog events. *Warm "Western V" conditions double the probability of EA droughts*. Approximately one-half (49%) of the 2016–18 versus one-quarter (26%) of the preindustrial simulations were dry (<–0.5Z). The simulations indicate that strong WVG conditions, produced by exceptionally (FAR = 1) warm WEP and WNP SST, doubled the chance of EA experiencing a drought in 2017. It should be noted, however, that this study relies on a single model. The National Academies recommends the use of a multimethod or multimodel approach (National Academies of Sciences 2016); as more large ensembles become available, this approach will be expanded. Here, we have shown that warm WV SST can produce EA drying on decadal (Fig. 1) and seasonal (Fig. 2) time scales. Enhanced early warning systems, risk reduction strategies, and climate services may help cope with these more frequent droughts.

ACKNOWLEDGMENTS. Support was provided by the USAID Famine Early Warning Systems Network and the U.S. Geological Survey Drivers of Drought program. Simulations were obtained from the ESRL Facility for Climate Assessments (FACTS) and the KNMI Climate Explorer. Reanalysis time series were obtained from the ESRL Web-based Reanalysis Intercomparison Toolkit (WRIT).

REFERENCES

Allen, M. R., 2003: Liability for climate change. *Nature*, **421**, 891–892, https://doi.org/10.1038/421891a.

FEWS NET, 2017a: Somalia: Persistent drought leads to major food security crisis. Famine Early Warning Systems Network, World Food Programme, accessed 23 March 2018, www.wfp.org/news/news-release/somalia-persistent-drought-leads-major-food-security-crisis-0.

——, 2017b: Decreases in staple food prices likely due to humanitarian assistance. Famine Early Warning Systems Network, World Food Programme, accessed 23 March 2018, http://fews.net/east-africa/somalia/key-message-update/march-2017.

Flato, G., and Coauthors, 2013: Evaluation of climate models. *Climate Change 2013: The Physical Science Basis*, T. F. Stocker et al., Eds., Cambridge University Press, 741–866.

FSNAU, 2017: Risk of Famine (IPC Phase 5) persists in Somalia. Food Security and Nutrition Analysis Unit–Somalia, accessed 23 March 2018, www.fsnau.org/in-focus/fewsnet-fsnau-joint-somalia-food-security-outlook-february-september-2017.

Funk, C., and A. Hoell, 2015: The leading mode of observed and CMIP5 ENSO-residual sea surface temperatures and associated changes in Indo-Pacific climate. *J. Climate*, **28**, 4309–4329, https://doi.org/10.1175/JCLI-D-14-00334.1.

——, and ——, 2017: Recent climate extremes associated with the west Pacific warming mode. *Climate Extremes: Patterns and Mechanisms*, S. Y. Wang et al., Eds., Wiley, 165–176, https://doi.org/10.1002/9781119068020.ch10.

——, and Coauthors, 2005: Recent drought tendencies in Ethiopia and equatorial–subtropical eastern Africa. Vulnerability to Food Insecurity: Factor Identification and Characterization Rep. 01/2005, FEWS NET, 12 pp., https://reliefweb.int/report/ethiopia/recent-drought-tendencies-ethiopia-vulnerability-food-insecurity-factor.

——, and Coauthors, 2013: Attribution of 2012 and 2003–12 rainfall deficits in eastern Kenya and southern Somalia [in "Explaining Extreme Events of 2012 from a Climate Perspective"]. *Bull. Amer. Meteor. Soc.*, **94**, 45–48, https://doi.org/10.1175/BAMS-D-13-00085.1.

——, S. Shukla, A. Hoell, and B. Livneh, 2015a: Assessing the contributions of East African and west Pacific warming to the 2014 boreal spring East African drought [in "Explaining Extreme Events of 2014 from a Climate Perspective"] *Bull. Amer. Meteor. Soc.*, **96**, S77–S82, https://doi.org/10.1175/BAMS-D-15-00106.1.

——, S. E. Nicholson, M. Landsfeld, D. Klotter, P. Peterson, and L. Harrison, 2015b: The Centennial Trends Greater Horn of Africa precipitation dataset. *Sci. Data*, **2**, 150050, https://doi.org/10.1038/sdata.2015.50.

——, and Coauthors, 2015c: The Climate Hazards Infrared Precipitation with Stations——A new environmental record for monitoring extremes. *Sci. Data*, **2**, 150066, https://doi.org/10.1038/sdata.2015.66.

——, and Coauthors, 2018: Examining the role of unusually warm Indo-Pacific sea surface temperatures in recent African droughts. *Quart. J. Roy. Meteor. Soc.*, https://doi.org/10.1002/qj.3266, in press.

Hoell, A., and C. Funk, 2014: Indo-Pacific sea surface temperature influences on failed consecutive rainy seasons over eastern Africa. *Climate Dyn.*, **43**, 1645–1660, https://doi.org/10.1007/s00382-013-1991-6.

——, M. Hoerling, J. Eischeid, X.-W. Quan, and B. Liebmann, 2017: Reconciling theories for human and natural attribution of recent East Africa drying. *J. Climate*, **30**, 1939–1957, https://doi.org/10.1175/JCLI-D-16-0558.1.

Huang, B., and Coauthors, 2015: Extended reconstructed sea surface temperature version 4 (ERSST. v4). Part

I: Upgrades and intercomparisons. *J. Climate*, **28**, 911–930, https://doi.org/10.1175/JCLI-D-14-00006.1.

Hurrell, J. W., and Coauthors, 2013: The Community Earth System Model: A framework for collaborative research. *Bull. Amer. Meteor. Soc.*, **94**, 1339–1360, https://doi.org/10.1175/BAMS-D-12-00121.1.

Liebmann, B., and Coauthors, 2014: Understanding recent eastern Horn of Africa rainfall variability and change. *J. Climate*, **27**, 8630–8645, https://doi.org/10.1175/JCLI-D-13-00714.1.

——, and Coauthors, 2017: Climatology and interannual variability of boreal spring wet season precipitation in the eastern Horn of Africa and implications for its recent decline. *J. Climate*, **30**, 3867–3886, https://doi.org/10.1175/JCLI-D-16-0452.1.

Lott, F. C., N. Christidis, and P. A. Stott, 2013: Can the 2011 East African drought be attributed to human-induced climate change? *Geophys. Res. Lett.*, **40**, 1177–1181, https://doi.org/10.1002/grl.50235.

Lyon, B., 2014: Seasonal drought in the Greater Horn of Africa and its recent increase during the March–May long rains. *J. Climate*, **27**, 7953–7975, https://doi.org/10.1175/JCLI-D-13-00459.1.

——, and D. G. DeWitt, 2012: A recent and abrupt decline in the East African long rains. *Geophys. Res. Lett.*, **39**, L02702, https://doi.org/10.1029/2011GL050337.

——, A. G. Barnston, and D. G. DeWitt, 2014: Tropical Pacific forcing of a 1998–1999 climate shift: Observational analysis and climate model results for the boreal spring season. *Climate Dyn.*, **43**, 893–909, https://doi.org/10.1007/s00382-013-1891-9.

National Academies of Sciences, 2016: *Attribution of Extreme Weather Events in the Context of Climate Change*. National Academies Press, 186 pp.

Newman, M., A. T. Wittenberg, L. Cheng, G. P. Compo, and C. A. Smith, 2018: The extreme 2015/16 El Niño, in the context of historical climate variability and change [in "Explaining Extreme Events of 2016 from a Climate Perspective"]. *Bull. Amer. Meteor. Soc.*, **99**, S16–S20, https://doi.org/10.1175/BAMS-D-17-0116.1.

Nicholson, S. E., 2014: A detailed look at the recent drought situation in the Greater Horn of Africa. *J. Arid Environ.*, **103**, 71–79, https://doi.org/10.1016/j.jaridenv.2013.12.003.

——, 2016: An analysis of recent rainfall conditions in eastern Africa. *Int. J. Climatol.*, **36**, 526–532, https://doi.org/10.1002/joc.4358.

——, 2017: Climate and climatic variability of rainfall over eastern Africa. *Rev. Geophys.*, **55**, 590–635, https://doi.org/10.1002/2016RG000544.

——, A. K. Dezfuli, and D. Klotter, 2012: A two-century precipitation dataset for the continent of Africa. *Bull. Amer. Meteor. Soc.*, **93**, 1219–1231, https://doi.org/10.1175/BAMS-D-11-00212.1.

Schneider, U., A. Becker, P. Finger, A. Meyer-Christoffer, M. Ziese, and B. Rudolf, 2014: GPCC's new land surface precipitation climatology based on quality-controlled in situ data and its role in quantifying the global water cycle. *Theor. Appl. Climatol.*, **115**, 15–40, https://doi.org/10.1007/s00704-013-0860-x.

Stott, P. A., D. A. Stone, and M. R. Allen, 2004: Human contribution to the European heatwave of 2003. *Nature*, **432**, 610–614, https://doi.org/10.1038/nature03089.

Sun, Q., C. Miao, Q. Duan, H. Ashouri, S. Sorooshian, and K.-L. Hsu, 2018: A review of global precipitation data sets: Data sources, estimation, and intercomparisons. *Rev. Geophys.*, **56**, 79–107, https://doi.org/10.1002/2017RG000574.

Uhe, P., and Coauthors, 2018: Attributing drivers of the 2016 Kenyan drought. *Int. J. Climatol.*, **38**, e554–e568, https://doi.org/10.1002/joc.5389.

Williams, P., and C. Funk, 2011: A westward extension of the warm pool leads to a westward extension of the Walker circulation, drying eastern Africa. *Climate Dyn.*, **37**, 2417–2435, https://doi.org/10.1007/s00382-010-0984-y.

Yang, W., R. Seager, M. A. Cane, and B. Lyon, 2014: The East African long rains in observations and models. *J. Climate*, **27**, 7185–7202, https://doi.org/10.1175/JCLI-D-13-00447.1.